HHS Public Access

Author manuscript

Nat Mater. Author manuscript; available in PMC 2019 September 25.

Published in final edited form as:

Nat Mater. 2019 July ; 18(7): 760–769. doi:10.1038/s41563-019-0323-6.

An integrin $\alpha_{IIb}\beta_3$ intermediate affinity state mediates biomechanical platelet aggregation

Yunfeng Chen[1,2,3,†], **Lining Arnold Ju**[2,4,5,6,7,†], **Fangyuan Zhou**[1,2], **Jiexi Liao**[2,4], **Lingzhou Xue**[8], **Qian Peter Su**[9], **Dayong Jin**[9], **Yuping Yuan**[5,6], **Hang Lu**[10], **Shaun P. Jackson**[3,5,6,*], and **Cheng Zhu**[1,2,4,5,*]

[1]Woodruff School of Mechanical Engineering, Georgia Institute of Technology, Atlanta, Georgia 30332, USA

[2]Petit Institute for Bioengineering and Biosciences, Georgia Institute of Technology, Atlanta, Georgia 30332, USA

[3]Department of Molecular Medicine, MERU-Roon Research Center on Vascular Biology, The Scripps Research Institute, La Jolla, California 92037, USA

[4]Coulter Department of Biomedical Engineering, Georgia Institute of Technology, Atlanta, Georgia 30332, USA

[5]Heart Research Institute, Mechanical and Mechatronic Engineering, The University of Sydney, Camperdown, NSW 2006, Australia

[6]Charles Perkins Centre, Mechanical and Mechatronic Engineering, The University of Sydney, Camperdown, NSW 2006, Australia

[7]School of Aerospace, Mechanical and Mechatronic Engineering, The University of Sydney, Camperdown, NSW 2006, Australia

[8]Department of Statistics, Pennsylvania State University, University Park, Pennsylvania 18602, USA

[9]Institute for Biomedical Materials and Devices (IBMD), Faculty of Science, University of Technology Sydney, Sydney, NSW, 2007, Australia

*Correspondence to Cheng Zhu (cheng.zhu@bme.gatech.edu) or Shaun Jackson (Shaun.Jackson@sydney.edu.au).
†These authors contributed equally.

Author contributions

Y.C. and L.A.J. designed and performed experiments, analyzed data and co-wrote the paper; F.Z., J.L. and Q.P.S. performed experiments and analyzed data; L.X. analyzed data and co-wrote the paper; Y.Y. provided critical suggestions and co-wrote the paper; D.J. co-supervised studies; H.L. provided critical devices and reagents; S.P.J. co-wrote the paper and co-supervised studies; C.Z. supervised the study, designed experiments and wrote the paper. Research activities related to this work were complied with relevant ethical regulations.

Competing Financial Interests

The authors have no conflict of interest to declare.

Reporting Summary

Further information on experimental design is available in the Reporting Summary.

Data availability

The data that support the findings of this study are available from the corresponding author upon reasonable request.

[10]School of Chemical & Biomolecular Engineering, Georgia Institute of Technology, Atlanta, Georgia 30332, USA.

Abstract

Integrins are membrane receptors mediating cell adhesion and mechanosensing. The structure-function relationship of integrins remains incompletely understood, despite the extensive studies due to its importance to basic cell biology and translational medicine. Using fluorescence dual biomembrane force probe, microfluidics and cone-and-plate rheometry, we applied precisely-controlled mechanical stimulations to platelets and identified an intermediate state of integrin $\alpha_{IIb}\beta_3$, which is characterized by an ectodomain conformation, ligand affinity and bond lifetimes that are all intermediate between the well-known inactive and active states. This intermediate state is induced by ligand engagement of GPIbα via a mechano-signaling pathway and potentiates the outside-in mechano-signaling of $\alpha_{IIb}\beta_3$ for further transition to the active state during integrin mechanical affinity maturation. Our work reveals distinct $\alpha_{IIb}\beta_3$ state transitions in response to biomechanical and biochemical stimuli, and identifies a role for the $\alpha_{IIb}\beta_3$ intermediate state in promoting biomechanical platelet aggregation.

Platelets participate in many physiological and pathological processes – hemostasis and thrombosis, immune responses, atherosclerosis, lymphatic vessel development, angiogenesis and tumor metastasis[1], most of which occur in a stressful mechanical milieu. To play such roles, platelets activate integrin $\alpha_{IIb}\beta_3$ to carry out adhesive and signaling functions[2-4]. Strikingly, platelets can rapidly sense and respond to hemodynamic forces to allow the mechanical environment to regulate their activation[4-7]. Disturbed blood flows, as occur with vessel stenosis or medical device intervention, stimulate platelet adhesion and aggregation, and facilitate the formation and propagation of thrombi[8,9], thereby increasing the risk of occlusive thrombosis[10]. The ability of platelets to sense hemodynamic forces largely depends on the mechanosensing of integrin $\alpha_{IIb}\beta_3$[9,11] and glycoproteins Ibα (GPIbα)[5,12-14] through their engaged ligands like fibrinogen (Fg), fibronectin and von Willebrand factor (VWF), although the detailed mechanisms remain incompletely understood.

Understanding how force stimulates platelet aggregation is clinically relevant, since the prothrombotic effects of disturbed blood flow cannot be eliminated by conventional antiplatelet agents that inhibit agonist-induced platelet aggregation mechanisms[8,10]. However, whether the $\alpha_{IIb}\beta_3$ integrins are activated similarly or differently by biomechanical versus biochemical (agonists, e.g., ADP, thrombin, TXA_2) stimuli is still elusive, hindering our understanding of the mechanisms underlying shear-induced thrombosis. Moreover, how GPIbα and $\alpha_{IIb}\beta_3$ interplay to coordinate platelet mechanosensing remains poorly defined.

Integrins are αβ heterodimers that have multiple states with distinct conformations and affinities. According to the switch-blade model[15], inactive integrins are bent (B) with closed headpiece (C) where the hybrid domain swings in; its ligand binding is undetectable until using ultrasensitive techniques[16]. Upon activation, integrins may unbend to an extended-closed (EC) conformation, followed by headpiece opening with hybrid domain swung-out, resulting in an extended-open (EO) conformation[17,18] (Fig. 1a). Integrin $\alpha_{IIb}\beta_3$ can be

activated bidirectionally, via inside-out signaling induced by GPIbα[19,20] or soluble agonist receptors[4], and outside-in signaling that requires ligand association[21]. The EO $\alpha_{IIb}\beta_3$ binds ligand with a high affinity[17,22]. In contrast, only standalone, unliganded EC $\alpha_{IIb}\beta_3$ was seen in crystal structures[23], which was hypothesized to have a low affinity similar to its BC conformer[24]. Nonetheless, whether EC $\alpha_{IIb}\beta_3$ exists physiologically, and if so, its function and regulation, are unclear.

By using our recently developed dual biomembrane force probe (dBFP)[20] and fluorescence biomembrane force probe (fBFP)[13] combined with microfluidic perfusion assays, we identified an intermediate affinity state of $\alpha_{IIb}\beta_3$ in EC conformation, which exists in and is critical to the development of biomechanical platelet aggregation. Furthermore, our work mapped the activation landscape of integrin $\alpha_{IIb}\beta_3$ on live platelets, and elucidated different mechanisms of $\alpha_{IIb}\beta_3$ activation in the development of biomechanical and biochemical thrombi.

Results

EC $\alpha_{IIb}\beta_3$ mediates biomechanical platelet aggregation

To investigate the role of $\alpha_{IIb}\beta_3$ activation in disturbed flow-induced platelet aggregation, we perfused human whole blood through a microfluidic channel with a two-dimension (2D) hump mimicking stenosis (Fig. 1b)[8,25]. Amplification loop blockers (ALB) was added to inhibit platelet activation by soluble agonists[26]. To define $\alpha_{IIb}\beta_3$ conformation and activation states, we used confocal microscopy to visualize real-time immunostaining of developing platelet aggregates by monoclonal antibodies (mAbs) (Fig. 1a). MBC370.2 recognizes a motif on the α_{IIb} Calf-1 domain only accessible on extended integrins[27]. AP5 recognizes an epitope in the β_3 PSI domain and reports hybrid domain swing-out[28]. Therefore, combined MBC370.2/AP5 staining defines the $\alpha_{IIb}\beta_3$ conformations: BC (MBC370.2$^-$/AP5$^-$), EC (MBC370.2$^+$/AP5$^-$) and EO (MBC370.2$^+$/AP5$^+$). PAC-1 binds the high-affinity form of $\alpha_{IIb}\beta_3$ ligand-binding site[29]. As a control, SZ22 stains all $\alpha_{IIb}\beta_3$ conformations[30].

Platelets aggregated downstream the hump primarily, which positively stained with MBC370.2 but not AP5 or PAC-1 (Fig. 1c; Supplementary Movies 1-3). The MBC370.2 staining requires stenosis shear stimulation, since it stained negative in the static condition (Supplementary Fig. 1).

To compare these results with biochemical platelet aggregation, we injected ADP (Fig. 1d) or thrombin receptor-activating peptide (TRAP) (Supplementary Fig. 2) 2 min after platelet aggregate formation. The chase of agonists rapidly increased the rate and extent of platelet aggregation, leading to channel occlusion, and generated extensive staining of MBC370.2, AP5 and PAC-1 (Supplementary Movies 4-6). The ADP- and TRAP-stimulated platelet aggregates displayed MBC370.2 staining comparable to, but AP5 and PAC-1 staining much higher than, biomechanically-induced platelet aggregates (all normalized by SZ22 staining) (Fig. 1e). Thus, on biomechanical platelet aggregates, a large portion of $\alpha_{IIb}\beta_3$ molecules were extended-closed and PAC-1 non-recognizable (PAC-1$^-$EC), whereas on biochemical platelet aggregates, many integrins were PAC-1$^+$EO. Corroborating this observation, a β_3

integrin extension reporter, MBC319.4[27], rendered similar staining as MBC370.2 (Supplementary Fig. 3).

Blocking GPIbα eliminated platelet aggregation (Fig. 1f,g; Supplementary Fig. 4a)[8], whereas blocking $\alpha_{IIb}\beta_3$ severely limited platelets from forming large and stable aggregates, notwithstanding the remaining platelets still stained with MBC370.2 (Fig. f,h; Supplementary Fig. 4b). Extending our previous discovery[8], These data indicate that biomechanical platelet aggregation is initiated by GPIbα and depends on $\alpha_{IIb}\beta_3$ with an EC conformation.

GPIbα mechano-signaling activates $\alpha_{IIb}\beta_3$ to EC conformation

To examine the GPIbα requirement of $\alpha_{IIb}\beta_3$ extension, we employed a dBFP adhesion frequency assay[20] to interrogate the interplay between GPIbα and $\alpha_{IIb}\beta_3$ on a single platelet. Probe I of the dBFP was functionalized with a recombinant VWF-A1 domain[31], which binds GPIbα but not $\alpha_{IIb}\beta_3$[32]; probe II was functionalized with a $\alpha_{IIb}\beta_3$ reporter mAb (Fig. 2a,b). We previously demonstrated that, a single GPIbα–A1 bond that sustains a 25-pN tensile force for >2-s suffices to trigger robust intraplatelet calcium[13] and upregulate $\alpha_{IIb}\beta_3$[20]. Therefore, we drove a micropipette-aspirated platelet to repeatedly touch probe I and retract to clamp at 25-pN. Once a >2-s lifetime event was observed (Supplementary Fig. 5a), the platelet was realigned to probe II to assess the resulting $\alpha_{IIb}\beta_3$ changes.

A1-stimulated platelets showed substantial binding to MBC370.2 and to another 'E'-conformation reporter, LIBS-2 (anti-β_3)[33], but not to AP5 or PAC-1, indicating that GPIbα mechano-signaling induces PAC-1$^-$EC $\alpha_{IIb}\beta_3$. In contrast, unstimulated platelets only adhered to the conformation-independent mAbs SZ22 and HIP8[34]; ADP-stimulated platelets adhered to all six mAbs at high frequencies (Fig. 2c). Thus, the same $\alpha_{IIb}\beta_3$ conformational changes were observed in the dBFP experiments as in the stenosis perfusion experiments, regardless of how such conformational changes were induced (mechanically or chemically).

The above results were confirmed by perfusing washed platelets through a microfluidic chamber co-functionalized with A1 and one of the mAbs (Fig. 2d). Platelet adhesion to A1/HIP8 and A1/LIBS-2 was high, but much lower to A1/AP5 and A1/PAC-1, which were significantly increased by ADP pre-treatment. Blocking GPIbα with 6D1 moderately decreased platelet adhesion on A1/HIP8, suggesting a minor contribution of GPIbα–A1 interaction to physically link platelets and the surface, but significantly reduced platelet adhesion on A1/LIBS-2, suggesting a crucial role for GPIbα–A1 interaction to induce $\alpha_{IIb}\beta_3$ extension.

Assessing integrin conformation by molecular stiffness

Force applied via an engaged ligand can lengthen the head-to-tail distance of an integrin as it behaves like a spring[35]. The integrin stiffness depends on its conformation, as extended integrins are stiffer than bent integrins[35] (Fig. 2e). We coated the dBFP probe II with a low-density of fibronectin module III domains 7–10 (abbreviated as FN) to pull $\alpha_{II}\beta_3$ for stiffness measurement one integrin per adhesion event[36]. On resting platelets, the measurements displayed a single-Gaussian histogram (Fig. 2f), which serves as benchmark stiffness for the BC integrins. After A1 stimulation by probe I, the integrin stiffness

histogram exhibited a broader shoulder on the right side of the peak, which is better-fitted (Methods; Supplementary Table 1) by a dual- than single-Gaussian distribution (Fig. 2g). The first Gaussian matched the BC $\alpha_{II}\beta_3$ stiffness in Figure 2f; the second subpopulation displayed a higher stiffness, suggesting the EC conformation. In contrast, the stiffness from ADP-stimulated platelets adopted a triple-Gaussian distribution (Supplementary Table 1; Fig. 2h). The first two subpopulations matched the stiffness of BC and EC $\alpha_{II}\beta_3$ molecules; the third subpopulation was likely contributed by EO $\alpha_{II}\beta_3$, with the further increased stiffness possibly resulting from the headpiece opening. Overall, our molecular stiffness measurements agree with the mAb mapping results. As a control, Mn^{2+} activation resulted in two subpopulations matching the stiffness of BC and EO, but not EC $\alpha_{II}\beta_3$ (Supplementary Fig. 5b).

EC $\alpha_{IIb}\beta_3$ binds ligand with an intermediate affinity

To characterize the ligand binding of EC $\alpha_{IIb}\beta_3$, we measured platelet adhesion frequency (P_a) to FN by dBFP. P_a was increased from 5% of resting platelets by A1 stimulation to 30%, which was further increased by ADP or thrombin to 70–80% (Fig. 3a). Chelating intracellular Ca^{2+} resulted in a lower P_a, whereas chelating extracellular Ca^{2+} had no effect (Supplementary Fig. 5c; Fig. 3a), confirming that GPIbα mechano-signaling requires intracellular but not extracellular calcium[5,6].

FN binds three platelet integrins with expression levels $\alpha_{IIb}\beta_3 >> \alpha_V\beta_3 \approx \alpha_5\beta_1$, all contributing to platelet adhesion[37-39]. To dissect the relative contributions of the three integrins to the measured P_a, we calculated the average number of total bonds bridging the platelet and the FN-bearing bead[36], $\langle n \rangle_{total} = -\ln(1 - P_a)$. Upon blocking $\alpha_V\beta_3$ with LM609[40] or $\alpha_{IIb}\beta_3$ with 10E5[41], we measured the remaining P_a and calculated the $\langle n \rangle_{total-\alpha V\beta 3}$ and $\langle n \rangle_{total-\alpha IIb\beta 3}$ ('–' meaning "minus"). After normalizing by the ligand density (m_l), we found $\langle n \rangle_{total-\alpha V\beta 3}/m_l + \langle n \rangle_{total-\alpha IIb\beta 3}/m_l$ indistinguishable from $\langle n \rangle_{total}/m_l$ for resting, A1-stimulated and ADP-stimulated platelets (Fig. 3b; Supplementary Table 2c). This suggests that the total bonds were primarily contributed by $\alpha_{IIb}\beta_3$ and $\alpha_V\beta_3$, which bind FN concurrently and independently[42]; whereas $\alpha_5\beta_1$ has negligible contribution, a conclusion confirmed by a β_3-inhibitor, integrilin[43], which eliminated all FN binding to the basal level (Supplementary Fig. 5c).

We next divided the $\langle n \rangle/m_l$ values by the surface densities of $\alpha_{IIb}\beta_3$ or $\alpha_V\beta_3$ (m_r) to calculate their average 2D effective affinities[36], $\langle A_c K_a \rangle$. Three levels of $\langle A_c K_a \rangle_{\alpha IIb\beta 3}$ were observed on resting, A1-stimulated and ADP-stimulated platelets (Fig. 3c). Considering A1 stimulation induces a subset of EC $\alpha_{IIb}\beta_3$ integrins, the higher $\langle A_c K_a \rangle_{\alpha IIb\beta 3}$ on A1-stimulated than resting platelets is attributed to a higher affinity of the EC $\alpha_{IIb}\beta_3$. A1- and ADP-stimulated platelets bound to 'E'-reporter mAbs at similar levels (Fig. 2c,d), indicating comparable surface densities of extended $\alpha_{IIb}\beta_3$ molecules (all EC on A1-stimulated and a EC/EO mixture on ADP-stimulated platelets). The higher $\langle A_c K_a \rangle_{\alpha IIb\beta 3}$ on ADP-stimulated than A1-stimulated platelets should therefore be attributed to a higher affinity of the EO than EC $\alpha_{IIb}\beta_3$. As a control, 0.5 mM Mn^{2+} elevated the $\langle A_c K_a \rangle_{\alpha IIb\beta 3}$ similar to A1 stimulation (Fig. 3c).

Using the same strategy, we found that platelet binding to Fg was also mediated by $\alpha_{IIb}\beta_3$ and $\alpha_V\beta_3$ (Fig. 3d,e; Supplementary Fig. 5c). Three levels of $<A_cK_a>_{\alpha IIb\beta3}$ were again observed on resting, A1-stimulated and ADP-stimulated platelets (Fig. 3c). Resting platelets have a much higher $<A_cK_a>_{\alpha IIb\beta3}$ for Fg than FN, agreeing with the previous reports that $\alpha_{IIb}\beta_3$ modulates resting platelets attachment to immobilized Fg but not fibronectin[44], likely owing to the distinct primary binding motifs (AGDV versus RGD) of the two ligands. The consistent results from two ligands demonstrated a hierarchy of affinities for the three $\alpha_{IIb}\beta_3$ conformations: BC < EC < EO.

EC $\alpha_{IIb}\beta_3$ dissociates from ligands with an intermediate rate

Dissociation rate under force is an important property of receptor–ligand interaction orthogonal to affinity. We used dBFP to measure single $\alpha_{IIb}\beta_3$–FN bond lifetimes – the reciprocal of dissociation rates (Fig. 4a). Resting platelets yielded a slip bond where the average lifetime decreased with force[45]. A1-stimulated platelets elicited a catch bond below 6.5 pN where the average lifetime increased with force[45], which turned into a slip bond over an extended force range; the average lifetimes were also longer across all forces. ADP stimulation greatly broadened the catch bond force regime, and further prolonged the lifetimes. Thus, the lifetimes of A1-stimulated platelets are between resting and ADP-stimulated platelets, correlating with the EC $\alpha_{IIb}\beta_3$. Using Fg also yielded three average lifetime curves that exhibit catch bonds (Fig. 4b), in contrast to the previous slip bond reports of purified $\alpha_{IIb}\beta_3$–Fg interactions[46,47] and suggesting the impact of the cellular environment. Together, these data demonstrated a hierarchy of force-dependent bond lifetimes for the three $\alpha_{IIb}\beta_3$ conformations: BC < EC < EO.

Notably, the GPIbα mechano-signaling induced intermediate state is specific for $\alpha_{IIb}\beta_3$. Although $\alpha_V\beta_3$ can be activated by ADP[38,48], it was unresponsive to GPIbα mechano-signaling (Fig. 3f; Supplementary Fig. 6a-e). Platelet $\alpha_5\beta_1$ could be activated by activating mAb TS2/16 or Mn^{2+} to bind FN, but not by A1- or ADP-stimulation (Supplementary Fig. 6f).

Besides binding to GPIbα, full-length VWF also binds $\alpha_{IIb}\beta_3$ via the RGD moiety. We found that GPIbα mechano-signaling is still the pre-requisite for $\alpha_{IIb}\beta_3$ to be intermediately activated for VWF binding (Supplemental Note 1).

Altogether, our results define an intermediate state for $\alpha_{IIb}\beta_3$ that features an EC conformation, intermediate ligand binding affinity and bond lifetime, distinguishing itself from the inactive and active states that respectively adopt the BC and EO conformations, low and high ligand binding affinities, and short and long bond lifetimes (Fig. 4c).

Distinct $\alpha_{IIb}\beta_3$ responses to different inside-out signals

Platelets stimulated by 2-μM ADP bound FN with a similar P_a as A1-stimulated platelets (Fig. 3a), but their lifetime curve was indistinguishable from that of 50-μM ADP-stimulated platelets (Fig. 4a), suggesting that low-dose ADP activates $\alpha_{IIb}\beta_3$ differently than A1. To further verify that mechanical and chemical stimulations (Fig. 5a) induce distinct $\alpha_{IIb}\beta_3$ inside-out signaling, we measured platelet dose-response to A1 and ADP stimulations using three complementary assays (all statistical analysis results summarized in Supplementary

Table 3). We define the “dose” of a mechanical stimulation as the amount/intensity of its mechanical effect.

We first used the dBFP to switch a platelet from an A1-probe to a FN- or Fg-probe to measure the $\alpha_{IIb}\beta_3$ adhesion frequency after the first GPIbα–A1 lifetime event, regardless of its duration. The post-switch P_a was found to increase with the A1 lifetime initially, indicating a mechanical dose-dependency of $\alpha_{IIb}\beta_3$ activation (Fig. 5b). The P_a then plateaued after 2 s and stayed unchanged for up to 60 s, confirming that the intermediate affinity was not due to insufficient mechanical stimulation. Replacing ligands with MBC370.2 yielded similar results; by comparison, the P_a to SZ22 was constantly high and those to AP5 and PAC-1 were at background levels, showing no dose-dependency (Fig. 5c).

We next employed a cone-and-plate rheometer to apply varied shear rates (0–10,000 s^{-1}) to platelets mixed with dimeric VWF-A1 (dA1), which crosslinked GPIbα on two platelets and exerted forces on them. The resulting $\alpha_{IIb}\beta_3$ activation was examined by flow cytometry with reporter mAbs. While the majority of platelets remained singlets (Supplementary Fig. 7a), the fraction of platelets positively stained by MBC370.2, but not AP5 or PAC-1, increased significantly with shear (Supplementary Fig. 7b-f; Fig. 5d), indicating a mechanical dose-dependency of the PAC-1^-EC $\alpha_{IIb}\beta_3$ population. In contrast, stimulation of ADP from 0.01 to 10 μM without shearing increased staining of all three reporter mAbs with statistically similar trends (Fig. 5e), indicating a dose-dependent increase of the PAC-1^+EO $\alpha_{IIb}\beta_3$ population.

We then used a ‘zoning’ microfluidic chamber, which recapitulates the dBFP switch assay in a high-throughput manner. FN, A1 and an $\alpha_{IIb}\beta_3$ reporter mAb were micro-patterned in three spatially adjacent zones (Fig. 5f). Platelet suspension was perfused to first flow through the FN-zone to confirm their unadherent resting state. The platelets then translocated on and were stimulated by the A1-zone whose length varied on different devices, providing adjustable doses of mechanical stimulation to platelets. Subsequently, platelets entered the mAb-zone to report $\alpha_{IIb}\beta_3$ status. The number of captured platelets on MBC370.2 increased initially with the A1-zone length and plateaued at 400 μm, whereas platelet capturing on SZ22 was uniformly high and on AP5 and PAC-1 uniformly low (Fig. 5g). In contrast, adhesion of ADP-stimulated platelets in a single-zone flow chamber to surfaces coated with MBC370.2, AP5 or PAC-1, but not SZ22, all increased dose-dependently (Fig. 5h).

The above three assays consistently demonstrated distinctive dose-dependencies of $\alpha_{IIb}\beta_3$ activation to both mechanical and chemical stimuli: GPIbα mechano-signaling only upregulated $\alpha_{IIb}\beta_3$ to the intermediate state, whereas ADP evoked the emergence of active $\alpha_{IIb}\beta_3$ even at low-doses. These different activation outcomes indicate distinct underlying signaling mechanisms.

Distinct signals following mechanical and chemical stimulations

The distinction in signaling mechanisms was further demonstrated by fBFP[13] showing distinctive intraplatelet Ca^{2+} patterns (transient vs. sustained) in A1- and ADP-stimulated platelets (Fig. 5i)[5,6]. Importantly, ADP- but not A1-triggered Ca^{2+} was suppressed by EGTA

(Fig. 5i-k), demonstrating different sources of Ca^{2+}: extracellular Ca^{2+} influx was involved during ADP stimulation, whereas A1 stimulation only triggered internal storage release[5,6].

From intermediate state to mechanical affinity maturation

We used the dBFP to study the interplay of integrin inside-out and outside-in signaling. After a >2-s A1 lifetime event, we measured post-switch $\alpha_{IIb}\beta_3$–FN and $\alpha_{IIb}\beta_3$–Fg binding over a prolonged time, which exerted repetitive intermittent mechanical stimulations to the integrins and monitored their binding changes concurrently. Remarkably, binding frequency displayed a sigmoidal time course, with the corresponding $<A_cK_a>$ plateauing at a level similar to that of ADP-stimulated platelets (Fig. 6a-c), suggesting integrin affinity maturation. This gradual elevation of integrin activity was not due to a delayed response to GPIbα mechano-signaling, because prolonging the A1-to-FN switch time interval yielded a gradual decay in the integrin activity (Supplementary Fig. 8a). Repeated pulling on integrins also triggered strong and sustained intraplatelet platelet Ca^{2+} (Fig. 6d-f) whose onset preceded integrin affinity maturation (Fig. 6a). No binding increase was observed when extracellular Ca^{2+} was chelated to eliminate the Ca^{2+} signaling (Fig. 6d-f) or when the platelet was touched continuously with a ligand-coated bead to allow bond formation and dissociation at zero-force for 5 min but without pulling (Fig. 6a,b). The data indicate that the affinity maturation requires both force on $\alpha_{IIb}\beta_3$ and extracellular Ca^{2+} influx[5,6] and rule out the contribution of ligand “priming”-induced integrin activation, which requires neither force nor cellular signaling[17,49]. The requirement of sequential GPIbα and $\alpha_{IIb}\beta_3$ mechano-signaling underscores the mechanical nature of this affinity maturation process. The results also reveal the transient nature of the intermediate state in the absence of sufficient stimulation.

Both the initial FN binding and its subsequent elevation over repetitive touches were suppressed by pre-treating platelets with BAPTA-AM, prolonging the A1-to-FN switch time interval or shortening the A1 lifetime (Fig. 6a; Supplementary Fig. 8). Without A1 pre-stimulation, $\alpha_{IIb}\beta_3$ remained at the low-activity level indicative of resting state (Fig. 6a-c) and did not trigger any Ca^{2+} above the baseline throughout the repetitive FN touches (Fig. 6d-f). These data indicate that GPIbα mechano-signaling that upregulates $\alpha_{IIb}\beta_3$ to the intermediate state is a pre-requisite for its mechanical affinity maturation.

To measure the $\alpha_{IIb}\beta_3$ lifetimes and molecular stiffness after mechanical affinity maturation (>100 cycles), the contact time was shortened to 0.1 s to lower the adhesion frequency to ~20% (cf. Supplementary Fig. 9a). The lifetime curves were comparable to those of ADP-stimulated platelets (Fig. 6g,h); however, 70.7% and 18.5% of the bonds displayed stiffness values matching EC and EO $\alpha_{IIb}\beta_3$ (Fig. 6i; Supplementary Table 1). These indicate that after mechanical affinity maturation, intermediate state $\alpha_{IIb}\beta_3$ still dominates ligand binding, yet a small fraction of integrins adopt the active state to prolong bond lifetimes. Such a composition of $\alpha_{IIb}\beta_3$ conformers should represent most of the platelets in biomechanical platelet aggregates (Fig. 1c), where both GPIbα and $\alpha_{IIb}\beta_3$ are engaged with ligands. Without extracellular Ca^{2+} or A1 pre-stimulation, the $\alpha_{IIb}\beta_3$ either returned to the inactive state or remained inactive despite repetitive ligand pulling (Fig. 6g,h,j,k).

Discussion

Our findings of the conformation-function relationship of integrin can be summarized in a model of $\alpha_{IIb}\beta_3$ activation and mechanosensing as related to platelet aggregation (Supplementary Fig. 10). On resting platelets, $\alpha_{IIb}\beta_3$ integrins exist in the inactive state incapable of supporting platelet aggregation. During biomechanical thrombus development, GPIbα mechano-signaling induces transient intracellular Ca^{2+} release and upregulates a large fraction of $\alpha_{IIb}\beta_3$ integrins to the intermediate state; subsequently, outside-in mechano-signaling of the intermediate state $\alpha_{IIb}\beta_3$ triggers sustained extracellular Ca^{2+} influx and promotes some of the integrins to the active state[17,50]. In contrast, in biochemical thrombus formation, ADP and thrombin trigger sustained Ca^{2+} and upregulate $\alpha_{IIb}\beta_3$ mainly to the active state. Both intermediate state and active state integrins have elevated affinities and prolonged bond lifetimes, thereby reinforcing thrombus growth. Future studies are required to further elucidate the signaling pathways underlie $\alpha_{IIb}\beta_3$ biomechanical and biochemical activation.

Due to the lack of relayed coupling between the αI-βI domains, αI-absent integrins were hypothesized to be unable to have a higher affinity in the EC than BC conformation[18,24]. We observed sustained expression of EC $\alpha_{IIb}\beta_3$ on live platelets that displays an intermediate affinity and bond lifetimes, demonstrating that EC $\alpha_{IIb}\beta_3$ is not merely a functionally “inert” state on the path of transitioning towards the EO conformation[17,23,50]. Interestingly, PAC-1 does not report $\alpha_{IIb}\beta_3$ intermediate activation (Supplementary Note 2).

Integrin affinity maturation describes the progression of integrin activation from the low to high affinity state. We showed that, without forming a cluster of integrin–ligand bonds (e.g., in focal adhesion), repetitive and intermittent ramp forces on single intermediate (but not inactive) state $\alpha_{IIb}\beta_3$ trigger mechanical outside-in signaling, resulting in affinity maturation. This extends our understanding of integrin-mediated mechanosensing[51-54]. The sequential GPIbα and $\alpha_{IIb}\beta_3$ mechano-signaling defines a mechanical pathway of integrin affinity maturation, where the integrin binding propensity increases with a continuing mechanical stimulation, which is different from the biochemical activation of $\alpha_{IIb}\beta_3$ by soluble agonists, and also from the reported affinity maturation in integrin $\alpha_L\beta_2$ on T lymphocytes produced by combined soluble agonist stimulation and immobilized-ligand binding[55]. Our data also suggests an ‘on/off’ switch of $\alpha_{IIb}\beta_3$ outside-in signaling: it will be switched ‘on’ only after $\alpha_{IIb}\beta_3$ adopts the intermediate state; otherwise, it remains ‘off’.

Biomechanical platelet thrombi formed in stenosed blood vessels were observed in multiple arterial injury models under disturbed blood flow[8], and primarily governed by the GPIbα-$\alpha_{IIb}\beta_3$ axis[5,6,19]. Considering the importance of mechano-signaling in varied stages of thrombus development (Supplementary Note 3), our findings that biomechanical thrombus growth is mainly mediated by intermediate state $\alpha_{IIb}\beta_3$ triggered by a biomechanical activation pathway will likely guide the development of new anti-thrombotic strategies.

Methods

Proteins, antibodies and reagents

Biotinylated FN was from Andres Garcia (Georgia Tech, Atlanta, GA). Recombinant monomeric and dimeric VWF 1208-A1 (residues A0742–17/21)[56] was from Zaverio Ruggeri (The Scripps Research Institute, La Jolla, CA). Human fibrinogen was purified from freshly frozen plasma using a described method[57]. Integrilin® or eptifibatide was from Millenium Pharmaceuticals (Cambridge, MA). mAbs 10E5 and 6D1 were from Barry Coller (Rockefeller University, New York, NY), AP5 from Peter Newman (BloodCenter of Wisconsin, Milwaukee, WI). ALMA12 from François Lanza (INSERM U.311, Strasbourg, France), HIP8-FITC, PAC-1 and isotype controls (H57 anti-mouse TCRβ) from BD Biosciences (San Jose, CA), LM609, ab62 (LIBS-2) and P1D6 from EMD Millipore (Billerica, MA), TS2/16 and unlabeled HIP8 from Thermo Fisher Scientific (Waltham, MA), SZ22 from Beckman Coulter (Brea, CA), MBC319.4 and MBC370.2[27,58] from Kerafast (Boston, MA), PAC-1-Alexa647 from BioLegend (San Diego, CA), Abciximab® (c7E3 Fab) from Eli Lilly (Indianapolis, IN), HFN 7.1 from Abcam (Cambridge, MA), 1D6 from Santa Cruz Biotechnology (Dallas, TX), and PE-conjugated polyclonal anti-mouse antibody from eBioscience (San Diego, CA). Conjugation of some mAbs with Alexa488 or Alexa647 was done using Zenon® Labeling Kit following the manufacturer instruction (Thermo Fisher Scientific).

Thrombin Receptor Activator Peptide (TRAP-6; SFLLRN, 4017752) was from Bachem (Bubendorf, Switzerland). Hirudin (Refludan) was from Pharmion/Celgene (Summit, NJ). Fura2-AM was from Thermo Fisher Scientific. ADP, thrombin, nystatin, streptavidin-maleimide (SA-MAL), dimethyl sulfoxide (DMSO), apyrase, theophylline, Clexane and bovine serum albumin (BSA) were from Sigma-Aldrich (St. Louis, MO). MAL-PEG3500-NHS and biotin-PEG3500-NHS were from JenKem (Plano, TX). Borosilicate glass beads were from Distrilab Particle Technology (RC Leusden, The Netherlands). All other reagents were from Sigma-Aldrich unless stated otherwise.

Blood collection, and platelet isolation and preparation

All procedures involving the collection of blood from healthy donors were approved by the University of Sydney Human Research Ethics Committee (HREC, Project 2014/244) and the Institutional Review Board of the Georgia Institute of Technology (protocol number H12354). All human donor blood samples were obtained with written informed consent. Blood was slowly drawn from the vein of a healthy volunteer. For whole blood perfusion studies, blood was anticoagulated with hirudin (800 U mL^{-1}). For platelet isolation, blood was drawn to fill in a 3 ml syringe preloaded with 0.43 ml ACD buffer (85 mM sodium citrate, 72.9 mM citric acid anhidrous, 110 mM D-glucose and 70 mM Theophylline, pH 4.6). Whole blood was transferred into a 15 ml tube pre-loaded with apyrase (0.005 U mL^{-1}) and Clexane (20 U mL^{-1}). After resting for 15 min at 37 ºC, whole blood was centrifuged at 200 g for 10 min without brake. Platelet-rich plasma was extracted, allowed to rest for 10 min at 37 ºC and centrifuged at 1,700 g for another 5 min. The platelet pellet was resuspended into platelet washing buffer (4.3 mM K_2HPO_4, 4.3 mM Na_2HPO_4, 24.3 mM NaH_2PO_4, 113 mM NaCl, 5.5 mM D-Glucose, 10 mM theophylline and 1% BSA, pH 6.5)

pre-added with Clexane (20 U mL^{-1}) and apyrase (0.01 U mL^{-1}), rested for 10 min and centrifuged again at 1,500 g for 5 min. The platelet pellet was resuspended into Hepes-Tyrode buffer (134 mM NaCl, 12 mM $NaHCO_3$, 2.9 mM KCl, 0.34 mM sodium phosphate monobasic, 5 mM HEPES, and 5 mM glucose, 1% BSA, pH 7.4) pre-added with apyrase (0.02 U mL^{-1}) with a platelet count at 3 ×10^8 mL^{-1}, read from a Sysmex KX-21N haematology analyser (Kobe, Japan), and placed in a 37 °C water bath for 30 min before use. For activation by ADP or thrombin in BFP or flow chamber experiments, the platelet suspension was incubated with ADP or thrombin for 15 min before experiment.

Whole blood perfusion through stenosis microfluidic channels

The PDMS microfluidic channel incorporating a 85 degree fixed micro-contraction geometry (Fig. 1b) was designed to mimic hemodynamics *in vivo* with severe stenosis (80%) as previously described[8,25,59]. This geometry exposes platelets to well-defined spatial shear gradients that induce aggregation. The dimensions of the channel in its straight section are 100 μm (width) ×130 μm (height).

Hirudinated (800 U mL^{-1}) whole blood was first incubated with the conformation-independent mAb (SZ22-Alexa488) and an $\alpha_{IIb}\beta_3$ reporter Ab (MBC370.2-, AP5- or PAC-1-Alexa647, 1 μg mL^{-1}) for 10 min, then perfused through the bare PDMS microfluidic channel for 10 min. A flow rate of 16 μL min^{-1} was chosen to produce a bulk shear rates of 1,800 s^{-1} to mimic the blood flow in small arteries/arterioles[8]. Blood was introduced via a 200 μL reservoir cut into the PDMS block at the channel inlet and flow was induced with a single syringe connected to the outlet and withdrawn by a PHD ULTRA™ pump (Harvard Apparatus). Platelet aggregation was monitored with combined dual-color confocal microscopy with concurrent DIC imaging (Nikon A1R confocal microscope with a 40x objective). Fluorescent images were captured using NIS software, Version 4 (Nikon, Japan). Blood flow was observed within a focal plane approximately 30 μm above the coverslip bottom of the channels. Fluorescently labeled platelet aggregates were quantitatively analyzed on a frame-by-frame basis off-line using ImageJ 1.50a (Fiji). To determine the region of global and activated platelet aggregates, the SZ22-Alexa488 and MBC370.2-Alexa647 channels were subject to respective intensity thresholding. To quantitate the integrin activation status, the staining intensities of SZ22, MBC319.4, MBC370.2, AP5 or PAC-1 in the 647 channel were measured in the same SZ22 thresholded region to calculate the intensity ratio.

To isolate the mechanical effects of blood flow from agonist induced platelet activation, we performed experiments involving mechanical stimulations in the presence of the canonical platelet amplification loops blockers (ALB) as previously described[8,25]: apyrase (1 U mL^{-1}), MRS2179 (100 mM) and 2-MeSAMP (10 mM) — to block ADP; indomethacin (10 μM)— to block TXA2; and hirudin (800 U mL^{-1})—to block thrombin. To investigate the agonist induced platelet activation, ADP (50 μM) or TRAP (500 μM) was injected to the microfluidic channel after 5 min perfusion of untreated whole blood.

In certain experiments, ALAM12 mAb (50 μg mL^{-1}) or Abciximab (20 μg mL^{-1}) was added to block platelet GPIbα or $\alpha_{IIb}\beta_3$ bindings respectively.

RBC and glass bead preparation for BFP experiments

Blood collections followed the protocol approved by the Institutional Review Board of the Georgia Institute of Technology after written informed consent was obtained from subjects. 8–10 μL of human blood was collected from finger prick and centrifuged to isolate RBCs. RBCs were biotinylated by incubating with Biotin-PEG3500-NHS (JenKem) solution[60] and partially swollen for BFP assembly by incubating with nystatin (Sigma-Aldrich).

The protocol of beads functionalization has been described[60]. Glass beads (Distrilab Particle Technology, Leusden, Netherlands) were first thiolated. To make FN beads, the thiolated glass beads were incubated first with SA-MAL overnight, then biotinylated FN for 3 h. The X0.1 and X3 FN beads were made by adjusting the FN incubation concentration to 0.1-fold or 3-fold, respectively. To make Fg, mA1, LIBS-2, HIP-8, PAC-1 or AP5 beads, the protein was first mixed and incubated with MAL-PEG3500-NHS (JenKem) for 30 min[31,61]. The mixture was then incubated with the thiolated glass beads overnight. Beads were washed with and resuspended in phosphate buffer (27.6 g/L $NaH_2PO_4 \cdot H_2O$, 28.4 g/L Na_2HPO_4).

BFP setups, experiment modes and related assays

Our first generation BFP setup and operation has been described[60]. Briefly, in an experimental chamber filled with Hepes-Tyrode buffer, a biotinylated RBC was aspirated by a micropipette with a probe bead attached to its apex via SA-biotin interaction, which forms a force transducer (Fig. 2a,b). The bead was functionalized with proteins of interest to interact with the receptors on the platelet aspirated by an opposing micropipette (Fig. 2a,b), which was driven by a piezoelectric translator (Physik Instrumente, Karlsruhe Germany) to move with a nano-meter resolution. The horizontal position of the probe bead was tracked by a high-speed camera, which reflected the RBC axial deformation and, by calculation, the platelet-bead force. The BFP spring constant k, determined using Evans' model[62], was set to 0.3 or 0.25 pN nm^{-1} for clamping forces higher or lower than 10 pN, respectively, by adjusting the aspirating pressure based on the measured diameters of the micropipette, spherical portion of the RBC and RBC-bead contacting area. Experimental data were collected and analyzed by LabView (National Instrument, Austin, TX). In the experimental chamber, 1 mM Ca^{2+}/Mg^{2+} or 1 mM Mg^{2+}/EGTA was added to provide or eliminate extracellular Ca^{2+} while maintaining integrin binding capability. In some experiments, ADP, thrombin, or 0.5 mM of Mn^{2+} was added to activate the platelet integrins. For experiments that did not activate the platelets, apyrase with a final concentration of 0.02 U mL^{-1} was added into the experimental chamber to chelate ADP released from the platelets.

Force-clamp mode and bond lifetime assay—Force-clamp mode was used to measure single receptor–ligand bond lifetimes under a range of constant forces. The probe bead ligand coating density was adjusted to keep the adhesion infrequent (<20%) to satisfy the necessary condition for most of the adhesions (>89%) to be single bond events[63]. The platelet was driven to contact and impinge the probe bead, and then retracted at 3 μm s^{-1}. When binding was detected during retraction, the target pipette was held at a pre-set force to wait for bond dissociation, and returned to the original position to start the next cycle (Supplementary Fig. 5a, Trace 3). Lifetime was defined as the duration of the clamping

phase before bond dissociation. Lifetime data were binned according to the clamp forces. The forces and lifetimes in each bin were then averaged to plot the lifetime vs. force curve.

In most platelet–FN lifetime measurements, FN was captured via its C-terminal biotin by wild-type (WT) tetravalent SA onto the BFP bead[64]. To exclude the possibility of multimeric bonds between up to four FN molecules captured by one SA and potential $\alpha_{IIb}\beta_3$ clusters, mutant monovalent SA was used in some experiments as control[64], which resulted in indistinguishable $\alpha_{IIb}\beta_3$–FN bond lifetimes under A1- and ADP-stimulated conditions (Fig. 4a). Because the higher the bond number the longer the lifetime[45], these data indicate that multimeric-bond effect was negligible using the WT SA.

Force-ramp mode and adhesion frequency assay—Force-clamp mode was used to detect the occurrence of adhesions at the end of a pre-set contact time for adhesion frequency assay, which allows for measurement of 2D receptor–ligand binding kinetics[36]. In a test cycle, the platelet approached and contacted the probe bead and retracted. A tensile force signal following retraction reports an adhesion event (Supplementary Fig. 5a, Trace 2) between the platelet and the bead, while the compressive force directly returning to zero indicated a no-adhesion event (Supplementary Fig. 5a, Trace 1). The approach-contact-retraction cycle was repeated for 30 times for 3 cell–bead pairs. The numbers of no-adhesion and adhesion events were enumerated to render a mean ± s.e.m. of adhesion frequency (P_a). Adhesion frequencies measured over a range of contact times contain information on both binding affinity and kinetics, whereas those measured at sufficiently long contact time (5 s) contain affinity information only as bond formation and dissociation have reached a dynamic equilibrium[36]. The 5-s contact time was used for measuring integrin–ligand binding affinities (Figs. 3 and 6b).

Dual BFP switch assay—The switch assay uses the dual BFP (dBFP) to analyze the crosstalk between cell surface receptors, as recently described[9,20]. The dBFP setup has two probes on one side for the same platelet to contact sequentially. The platelet was first aligned to probe I coated with VWF A1 (Fig. 2a) and tested by repeated cycles using force-clamp mode at 25 pN. Once a lifetime event of any duration (Fig. 5b, c) or >2 s (other figures) was observed, the platelet-aspirating micropipette was manually switched (within <30 s) to align with probe II coated with FN, Fg, or an anti-$\alpha_{IIb}\beta_3$ mAb (Fig. 2b) depending on whether the experimental objective was to measure ligand binding or conformation or activation state of $\alpha_{IIb}\beta_3$. Force-ramp or -clamp mode was used depending on whether the desired type of assay was adhesion frequency or bond lifetime.

Fluorescence BFP assay for concurrent intracellular Ca^{2+} imaging—We used fBFP to quantify intraplatelet Ca^{2+} level induced by GPIbα mechano-signaling or agonist receptor signaling, as previously described[13,65]. All results were obtained from $n \geq 3$ independent experiments in duplicates.

We pre-incubated platelets with Fura2-AM and analyzed one platelet at a time by concurrent force spectroscopy and Ca^{2+} imaging for a continuous period of 200 s. The force spectroscopic assays were done in either force-ramp or force-clamp mode using either a single force probe or dual force probes[20]. Calcium was measured using ratiometric imaging

with a light source that alternates two excitation wavelengths, 340 and 380 nm to excite Ca^{2+}-bound and -free Fura2, respectively. The two emission lights were captured by a fluorescence camera[13,65]. The real-time intracellular Ca^{2+} level over the 200-s observation time was quantified by the ratio of the emissions excited by the 340 and 380 nm channels collected by the software Micromanager (Version 1.4), which was normalized by the initial value.

The Ca^{2+} time curve was quantified by two parameters: maximum Ca^{2+} intensity increase, ΔI_{max}, and area-under-curve, AUC. ΔI_{max} was defined as the maximal amplitude of the signal elevation over the 200-s observation time. AUC was calculated as the total area of signal elevation of the 'Normalized Ca^{2+} intensity vs. time' curve (e.g., Figs. 5i & 6d) divided by 200 s[65].

Molecular stiffness measurement

As previously described[35], the stiffness of a single integrin–ligand complex was measured by the stretch method using the ramp phase data of the BFP experiment (Supplementary Fig. 5a). The force vs. time data were transformed using the displacement vs. time data, which were read from the capacitive strain sensor of the piezoelectric translator that drove the platelet holding micropipette. The resulting force vs. displacement data were fit to two line segments with a kink at the zero force point (Supplementary Fig. 9b). The slope of the compressive segment (force <0) reflects the stiffness of the platelet, denoted by a spring constant k_{plt} (Supplementary Fig. 9c). The slope of the tensile segment (force >0) reflects the stiffness of the platelet and the ligand–ligand complex in series, denoted by an equivalent spring constant k_{eq}. The molecular stiffness, denoted by a spring constant k_{mol}, can be calculated as $k_{mol} = (1/k_{eq} - 1/k_{plt})^{-1}$ (Supplementary Fig. 9c). The k_{mol} value mainly reflects the integrin stiffness as the contribution from FN is negligible.

To measure integrin stiffness, probe II of dBFP was coated with FN with a titrated density to ensure infrequent adhesion (≤20%) under each condition. To measure stiffness of $\alpha_{IIb}\beta_3$, mAb LM609 was added to block $\alpha_V\beta_3$ binding. To measure stiffness of $\alpha_V\beta_3$, mAb 10E5 was added to block $\alpha_{IIb}\beta_3$ binding. In control experiments, integrilin was added to test binding specificity, which eliminated almost all adhesion events under all conditions, indicating no contribution from $\alpha_5\beta_1$ binding.

Similar to the control experiments performed for lifetime measurements, to exclude the possibility of multimeric bonds between up to four FN molecules captured by SA and potential $\alpha_{IIb}\beta_3$ clusters, molecular stiffness was also measured with mutant monovalent SA, which rendered no significant difference (Supplementary Fig. 9d). This again indicated that multimeric-bond effect was negligible using the WT SA.

Molecular site density measurement

We used flow cytometry to measure receptor and ligand site densities on platelets and BFP beads, respectively, as previously described[36]. Platelets were incubated with a FITC-conjugated HIP-8 at 10 μg mL^{-1} at room temperature for 30 min for $\alpha_{IIb}\beta_3$ site density (m_r) measurement, or incubated first with LM609 at 10 μg mL^{-1} for 30 min and then PE-conjugated anti-mouse antibody for 30 min for $\alpha_V\beta_3$ m_r measurement. The m_r values were

measured using conformation-independent mAbs, hence including all conformers. The FN and Fg coated beads were incubated first with HFN 7.1 and 1D6 (Santa Cruz Biotechnology), respectively, and then with a PE-conjugated polyclonal anti-mouse antibody. The fluorescent intensities of the cells or beads were measured by a BD LSR flow cytometer (BD Biosciences), and compared to standard calibration beads (Bangs Laboratories, Fishers, IN) to determine the number of molecules per cell/bead. The site density was calculated by dividing the total number of molecules per cell/bead to the cell/bead surface area[36], which was calculated from the radii measured with a customized Labview (National Instrument) program.

Calculation of average affinity

For biomolecular interaction between two molecular species, the equilibrium adhesion frequency can be related to the average number of receptor–ligand bonds by $<n> = -\ln(1 - P_a) = m_r m_l A_c K_a$ based on our published model[36], where, m_r and m_l are respective site densities of receptors (measured using conformation-independent mAbs) and ligands which are measured by immunostaining and flow cytometry, A_c is the contact area and K_a is the affinity in μm^2. However, platelets express three FN-binding integrins. Also, different copies of the same integrin may exist in different affinity states. Therefore, the average number of total bonds $<n>_{total} = <n>_1 + <n>_2 + \ldots$ if the concurrent interactions of different species are independent, where $<n>_i = m_{r,i} m_{l,i} A_c K_{a,i}$ is the average number of bonds of the ith molecular species expressing in terms of their site densities and affinity[66] For example, the $\alpha_{IIb}\beta_3$ site density m_r on ADP-activated platelets included three fractions ($f_i = m_{r,i}/m_r$, $i = 1$–3) with low ($K_{a,1}$), intermediate ($K_{a,2}$) and high ($K_{a,3}$) affinities for FN, coated on the BFP bead at a site density m_l. The adhesion frequency assay measures an average affinity that equals to the sum of the three affinities weighted by the three $\alpha_{IIb}\beta_3$ fractions:

$$< A_c K_a > = \frac{< n >_{total}}{m_l m_r} = \frac{< n >_1 + < n >_2 + < n >_3}{m_l m_r} = \frac{\sum_{i=1}^{3} m_{r,i} m_l A_c K_{a,i}}{m_l m_r} = A_c \sum_{i=1}^{3} f_i K_{a,i} \quad \text{(Equation 1)}$$

Note: When calculating $<n>$ (Fig. 3b) and $<A_c K_a>$ (Fig. 3c, f), binding of the FN beads used in Figure 3a was too low under certain conditions, which could overestimate the results. To allow accurate calculation, we repeated the experiments using beads with a higher FN coating density to ensure the adhesion frequency to reach a reasonable level (~20%) and to contain mostly specific binding.

Cone-and-plate shear assay

Isolated human platelets in Tyrode buffer (50×10^6 mL^{-1}) were gently incubated with dA1 (2 $\mu g\ mL^{-1}$) and desired $\alpha_{IIb}\beta_3$ conformation reporter mAbs (1 $\mu g\ mL^{-1}$) at 37°C for 10 min, then transferred to the stationary plate surface of a Kinexus Ultra+ rheometer (Malvern

Instruments, Malvern, UK). Shear rates were varied from 0 to 10,000 s^{-1}. During shear application, platelets were kept under humidified conditions at 37°C with an Active Hood Peltier Plate Cartridge. After shear stimulation of 5 min, ~50 μL platelet mixture was collected and immediately analyzed by flow cytometry.

Determination of agonist-stimulated integrin conformations by flow cytometry

Isolated platelets (50×10^6 mL^{-1}) in 100 μL Tyrode's buffer were stimulated with ADP (0–10 μM) for 10 min in the presence of desired $\alpha_{IIb}\beta_3$ reporter mAbs (1 μg mL^{-1}). Platelets were then diluted by 10 times to stop reaction and immediately analyzed by flow cytometry. The percentage of positive population and fluorescent intensities (Geomean) were analyzed using the FlowJo software (FlowJo LLC; Ashland, OR, USA). By default, the gate is set around the 2% position in the fluorescence intensity histogram of the corresponding isotype control.

Parallel flow chamber experiments using microfluidic devices

Single-zone setup—Microfluidic devices were uniformly coated with a solution of one or a mixture of two proteins (A1 and/or FN, 100 μg mL^{-1} each) for 1 h. The coated area is named reporting zone.

Multi-zone setup—The multi-zone device separates the ligand interaction with platelet GPIbα and integrin $\alpha_{IIb}\beta_3$ in space and time. In such devices, the flow chamber floor is divided into multiple functional zones, which are fabricated to register sequentially[67]. Platelets are perfused at 4 dynes/cm^2 to sequentially encounter each of them with spatiotemporal control, including: Zone A, B and C (Fig. 5d). Coating of the three zones was nearly seamless, leaving no gap between adjacent zones. Zone A was 800 μm long and coated with 100 μg mL^{-1} FN for 1 h. Zone B had a variable length of 50–800 μm and was coated with 100 μg mL^{-1} A1 for 1 h. Zone C was 800 μm long and was coated with 100 μg mL^{-1} of one of the $\alpha_{IIb}\beta_3$ reporter mAbs for 1 h.

Experiment procedure—Washed platelets (1×10^8 ml^{-1}) were perfused through the devices, and the number of adherent platelets per unit area in the reporting zone was counted on 2 random fields of view after 2 min of continuous flow. Each condition was repeated in 3 devices for each sample. For conditions that required ADP activation, platelet suspension was pre-incubated with ADP of varying concentrations (0.01, 0.1, 1, 10 μM) for 15 min before perfusing through the devices.

Statistical Analysis

For most experiments, statistical significance was assessed by two-tailed Student's t-test (statistics summarized in Supplementary Table 2).

For comparisons of goodness-of-fitting between single-, dual- and triple-Gaussian fits for the stiffness histograms, extra sum-of-squares F test (Supplementary Table 1a) and Akaike's information criteria (Supplementary Table 1b) were used.

To test signal-dose dependencies in Figure 5, we first performed the one-way analysis of variance (ANOVA) to examine the difference among signals corresponding to different

doses of the biomechanical or biochemical treatment (Supplementary Table 3a). When the ANOVA shows a significant difference, the Kendall's rank correlation[68] was used to test the positive dependency between signal and dose (Supplementary Table 3b), which has the advantage over Pearson's correlation in that it does not assume the curves to be linearly fitted.

To test whether the curves of MBC370, PAC-1 and AP5 in Figures 5e (*right*) and 5h follow the same trend, Chow test[69] was used to examine whether the curves adopt different linear regression models (Supplementary Table 3b). Due to the limited number of doses, more complicated statistical comparisons not assuming linear regression were not favored for use in these cases.

Supplementary Material

Refer to Web version on PubMed Central for supplementary material.

Acknowledgements

We thank A. Garcia (Georgia Tech), Z. Ruggeri (The Scripps Research Institute), B. Coller (Rockefeller University), P. Newman, R. Aster, J. Zhu and D. Bougie (BloodCenter of Wisconsin), W. Lam (Emory University) and F. Tovar Lopez (RMIT University) for providing precious reagents. We thank Y. Sakurai, D. Myer, Y. Qiu, R. Tran and J. Ciciliano from W. Lam lab (Georgia Tech) for the blood collection; R. Darbousset for support on platelet isolation and flow cytometry; A. Samson (WEHI) and J. Maclean (HRI) for cone-and-plate rheometry training; I. Alwis (USYD) for support on confocal microscopy; N. Court and E. Ilagan (USYD ANFF Research & Prototype Foundry) for advice on stenosis microchannel fabrication and characterization; S. Schoenwaelder (USYD), J. McFadyen (Baker Institute) and Z. Li (QUT) for helpful discussion.

This work was supported by grants from the NIH (HL1320194 - C.Z.; R21EB020424 - H.L.), the NSF (DMS-1505256; DMS-1811552 - L.X.), the NIDA (P50 DA039838 - L.X.), the NHMRC (APP1028564; APP1048574 - S.P.J.), the Australian Research Council (LE120100043 - S.P.J.), the University of Technology Sydney's Grant for IBMD (Q.P.S), the Diabetes Australia Research Program General Grant (G179720), the University of Sydney Early-Career Researcher Kickstart Grant and Cardiovascular Initiative Catalyst Grant for Precision CV Medicine, the Royal College of Pathologists of Australasia Kanematsu research award and the Cardiac Society of Australia and New Zealand BAYER Young Investigator Research Grant (L.A.J.). S.P.J. is an NHMRC Senior Principal Research Fellow. L.A.J. is an Australian Research Council DECRA fellow (DE190100609) and a former National Heart Foundation of Australia postdoctoral fellow (101798).

References

1. Xu XR et al. Platelets are versatile cells: New discoveries in hemostasis, thrombosis, immune responses, tumor metastasis and beyond. Critical reviews in clinical laboratory sciences 53, 409–430, doi:10.1080/10408363.2016.1200008 (2016). [PubMed: 27282765]
2. Shen B et al. A directional switch of integrin signalling and a new anti-thrombotic strategy. Nature 503, 131–135, doi:10.1038/nature12613 (2013). [PubMed: 24162846]
3. Stalker TJ et al. Hierarchical organization in the hemostatic response and its relationship to the platelet-signaling network. Blood 121, 1875–1885, doi:10.1182/blood-2012-09-457739 (2013). [PubMed: 23303817]
4. Li Z, Delaney MK, O'Brien KA & Du X Signaling during platelet adhesion and activation. Arteriosclerosis, thrombosis, and vascular biology 30, 2341–2349, doi:10.1161/ATVBAHA.110.207522 (2010).
5. Mazzucato M, Pradella P, Cozzi MR, De Marco L & Ruggeri ZM Sequential cytoplasmic calcium signals in a 2-stage platelet activation process induced by the glycoprotein Ibalpha mechanoreceptor. Blood 100, 2793–2800, doi:10.1182/blood-2002-02-0514 (2002). [PubMed: 12351387]

6. Nesbitt WS et al. Distinct glycoprotein Ib/V/IX and integrin alpha IIbbeta 3-dependent calcium signals cooperatively regulate platelet adhesion under flow. The Journal of biological chemistry 277, 2965–2972, doi:10.1074/jbc.M110070200 (2002). [PubMed: 11713259]
7. Kroll MH, Hellums JD, McIntire LV, Schafer AI & Moake JL Platelets and shear stress. Blood 88, 1525–1541 (1996). [PubMed: 8781407]
8. Nesbitt WS et al. A shear gradient-dependent platelet aggregation mechanism drives thrombus formation. Nature Medicine 15, 665–673, doi:10.1038/nm.1955 (2009).
9. Ju L et al. Compression force sensing regulates integrin alphaIIbbeta3 adhesive function on diabetic platelets. Nature communications 9, 1087, doi:10.1038/s41467-018-03430-6 (2018).
10. Jackson SP Arterial thrombosis--insidious, unpredictable and deadly. Nature Medicine 17, 1423–1436, doi:10.1038/nm.2515 (2011).
11. Goncalves I, Nesbitt WS, Yuan Y & Jackson SP Importance of temporal flow gradients and integrin alphaIIbbeta3 mechanotransduction for shear activation of platelets. The Journal of biological chemistry 280, 15430–15437, doi:10.1074/jbc.M410235200 (2005). [PubMed: 15701653]
12. Chen Y, Ruggeri ZM & Du X 14–3-3 proteins in platelet biology and glycoprotein Ib-IX signaling. Blood 131, 2436–2448, doi:10.1182/blood-2017-09-742650 (2018). [PubMed: 29622550]
13. Ju L, Chen Y, Xue L, Du X & Zhu C Cooperative unfolding of distinctive mechanoreceptor domains transduces force into signals. eLife 5, e15447, doi:10.7554/eLife.15447 (2016). [PubMed: 27434669]
14. Deng W et al. Platelet clearance via shear-induced unfolding of a membrane mechanoreceptor. Nature communications 7, 12863, doi:10.1038/ncomms12863 (2016).
15. Luo BH, Carman CV & Springer TA Structural basis of integrin regulation and signaling. Annual review of immunology 25, 619–647, doi:10.1146/annurev.immunol.25.022106.141618 (2007).
16. Zhang F et al. Two-dimensional kinetics regulation of alphaLbeta2-ICAM-1 interaction by conformational changes of the alphaL-inserted domain. The Journal of biological chemistry 280, 42207–42218, doi:10.1074/jbc.M510407200 (2005). [PubMed: 16234238]
17. Xiao T, Takagi J, Coller BS, Wang JH & Springer TA Structural basis for allostery in integrins and binding to fibrinogen-mimetic therapeutics. Nature 432, 59–67, doi:10.1038/nature02976 (2004). [PubMed: 15378069]
18. Li J & Springer TA Energy landscape differences among integrins establish the framework for understanding activation. The Journal of cell biology 217, 397–412, doi:10.1083/jcb.201701169 (2017). [PubMed: 29122968]
19. Kasirer-Friede A et al. Signaling through GP Ib-IX-V activates alpha IIb beta 3 independently of other receptors. Blood 103, 3403–3411, doi:10.1182/blood-2003-10-3664 (2004). [PubMed: 14726383]
20. Ju L et al. Dual Biomembrane Force Probe enables single-cell mechanical analysis of signal crosstalk between multiple molecular species. Scientific reports 7, 14185, doi:10.1038/s41598-017-13793-3 (2017). [PubMed: 29079742]
21. Durrant TN, van den Bosch MT & Hers I Integrin alphaIIbbeta3 outside-in signaling. Blood, doi:10.1182/blood-2017-03-773614 (2017).
22. Zhu J, Zhu J & Springer TA Complete integrin headpiece opening in eight steps. The Journal of cell biology 201, 1053–1068, doi:10.1083/jcb.201212037 (2013). [PubMed: 23798730]
23. Zhu J et al. Closed headpiece of integrin alphaIIbbeta3 and its complex with an alphaIIbbeta3-specific antagonist that does not induce opening. Blood 116, 5050–5059, doi:10.1182/blood-2010-04-281154 (2010). [PubMed: 20679525]
24. Springer TA & Dustin ML Integrin inside-out signaling and the immunological synapse. Current opinion in cell biology 24, 107–115, doi:10.1016/j.ceb.2011.10.004 (2012). [PubMed: 22129583]
25. Tovar-Lopez FJ et al. An investigation on platelet transport during thrombus formation at micro-scale stenosis. PloS one 8, e74123, doi:10.1371/journal.pone.0074123 (2013). [PubMed: 24194822]
26. Jackson SP, Nesbitt WS & Westein E Dynamics of platelet thrombus formation. Journal of thrombosis and haemostasis 7 Suppl 1, 17–20, doi:10.1111/j.1538-7836.2009.03401.x (2009). [PubMed: 19630759]

27. Zhang C et al. Modulation of integrin activation and signaling by alpha1/alpha1'-helix unbending at the junction. Journal of Cell Science 126, 5735–5747, doi:10.1242/jcs.137828 (2013). [PubMed: 24144695]
28. Cheng M, Li J, Negri A & Coller BS Swing-out of the beta3 hybrid domain is required for alphaIIbbeta3 priming and normal cytoskeletal reorganization, but not adhesion to immobilized fibrinogen. PloS one 8, e81609, doi:10.1371/journal.pone.0081609 (2013). [PubMed: 24349096]
29. Ye F, Kim C & Ginsberg MH Reconstruction of integrin activation. Blood 119, 26–33, doi: 10.1182/blood-2011-04-292128 (2012). [PubMed: 21921044]
30. Bassler N et al. A mechanistic model for paradoxical platelet activation by ligand-mimetic alphaIIb beta3 (GPIIb/IIIa) antagonists. Arteriosclerosis, thrombosis, and vascular biology 27, e9–15, doi: 10.1161/01.ATV.0000255307.65939.59 (2007).
31. Butera D et al. Autoregulation of von Willebrand factor function by a disulfide bond switch. Science advances 4, eaaq1477, doi:10.1126/sciadv.aaq1477 (2018). [PubMed: 29507883]
32. Ruggeri ZM & Mendolicchio GL Adhesion mechanisms in platelet function. Circulation research 100, 1673–1685, doi:10.1161/01.RES.0000267878.97021.ab (2007). [PubMed: 17585075]
33. Du X et al. Long range propagation of conformational changes in integrin alpha IIb beta 3. The Journal of biological chemistry 268, 23087–23092 (1993). [PubMed: 7693683]
34. McCarty OJ, Mousa SA, Bray PF & Konstantopoulos K Immobilized platelets support human colon carcinoma cell tethering, rolling, and firm adhesion under dynamic flow conditions. Blood 96, 1789–1797 (2000). [PubMed: 10961878]
35. Chen W, Lou J, Evans EA & Zhu C Observing force-regulated conformational changes and ligand dissociation from a single integrin on cells. The Journal of cell biology 199, 497–512, doi:10.1083/jcb.201201091 (2012). [PubMed: 23109670]
36. Chesla SE, Selvaraj P & Zhu C Measuring two-dimensional receptor-ligand binding kinetics by micropipette. Biophysical journal 75, 1553–1572, doi:10.1016/S0006-3495(98)74074-3 (1998). [PubMed: 9726957]
37. Bennett JS, Berger BW & Billings PC The structure and function of platelet integrins. Journal of Thrombosis and Haemostasis 7, 200–205, doi:DOI 10.1111/j.1538-7836.2009.03378.x (2009). [PubMed: 19630800]
38. McCarty OJ et al. Evaluation of the role of platelet integrins in fibronectin-dependent spreading and adhesion. Journal of thrombosis and haemostasis 2, 1823–1833, doi:10.1111/j.1538-7836.2004.00925.x (2004). [PubMed: 15456495]
39. Savage B, Almus-Jacobs F & Ruggeri ZM Specific synergy of multiple substrate-receptor interactions in platelet thrombus formation under flow. Cell 94, 657–666 (1998). [PubMed: 9741630]
40. Kaul DK et al. Monoclonal antibodies to alphaVbeta3 (7E3 and LM609) inhibit sickle red blood cell-endothelium interactions induced by platelet-activating factor. Blood 95, 368–374 (2000). [PubMed: 10627437]
41. Mitchell WB et al. Mapping early conformational changes in alphaIIb and beta3 during biogenesis reveals a potential mechanism for alphaIIbbeta3 adopting its bent conformation. Blood 109, 3725–3732, doi:10.1182/blood-2006-11-058420 (2007). [PubMed: 17209052]
42. Zhu C & Williams TE Modeling concurrent binding of multiple molecular species in cell adhesion. Biophysical journal 79, 1850–1857, doi:10.1016/S0006-3495(00)76434-4 (2000). [PubMed: 11023890]
43. Lele M, Sajid M, Wajih N & Stouffer GA Eptifibatide and 7E3, but not tirofiban, inhibit alpha(v)beta(3) integrin-mediated binding of smooth muscle cells to thrombospondin and prothrombin. Circulation 104, 582–587 (2001). [PubMed: 11479257]
44. Savage B, Shattil SJ & Ruggeri ZM Modulation of platelet function through adhesion receptors. A dual role for glycoprotein IIb-IIIa (integrin alpha IIb beta 3) mediated by fibrinogen and glycoprotein Ib-von Willebrand factor. The Journal of biological chemistry 267, 11300–11306 (1992). [PubMed: 1597464]
45. Marshall BT et al. Direct observation of catch bonds involving cell-adhesion molecules. Nature 423, 190–193, doi:10.1038/nature01605 (2003). [PubMed: 12736689]

46. Litvinov RI et al. Dissociation of bimolecular alphaIIbbeta3-fibrinogen complex under a constant tensile force. Biophysical journal 100, 165–173, doi:10.1016/j.bpj.2010.11.019 (2011). [PubMed: 21190668]

47. Litvinov RI et al. Resolving two-dimensional kinetics of the integrin alphaIIbbeta3-fibrinogen interactions using binding-unbinding correlation spectroscopy. The Journal of biological chemistry 287, 35275–35285, doi:10.1074/jbc.M112.404848 (2012). [PubMed: 22893701]

48. Bennett JS, Chan C, Vilaire G, Mousa SA & DeGrado WF Agonist-activated alphavbeta3 on platelets and lymphocytes binds to the matrix protein osteopontin. The Journal of biological chemistry 272, 8137–8140 (1997). [PubMed: 9079626]

49. Du XP et al. Ligands "activate" integrin alpha IIb beta 3 (platelet GPIIb-IIIa). Cell 65, 409–416 (1991). [PubMed: 2018974]

50. Xu XP et al. Three-Dimensional Structures of Full-Length, Membrane-Embedded Human alpha(IIb)beta(3) Integrin Complexes. Biophysical journal 110, 798–809, doi:10.1016/j.bpj.2016.01.016 (2016). [PubMed: 26910421]

51. Wang N Cellular adhesion: Instant integrin mechanosensing. Nature materials 16, 1173–1174, doi:10.1038/nmat5041 (2017). [PubMed: 29170552]

52. Humphrey JD, Dufresne ER & Schwartz MA Mechanotransduction and extracellular matrix homeostasis. Nature reviews. Molecular cell biology 15, 802–812, doi:10.1038/nrm3896 (2014). [PubMed: 25355505]

53. Irianto J, Pfeifer CR, Xia Y & Discher DE SnapShot: Mechanosensing Matrix. Cell 165, 1820–1820 e1821, doi:10.1016/j.cell.2016.06.002 (2016). [PubMed: 27315485]

54. Chen Y, Ju L, Rushdi M, Ge C & Zhu C Receptor-mediated cell mechanosensing. Molecular biology of the cell 28, 3134–3155, doi:10.1091/mbc.E17-04-0228 (2017). [PubMed: 28954860]

55. Schurpf T & Springer TA Regulation of integrin affinity on cell surfaces. The EMBO journal 30, 4712–4727, doi:10.1038/emboj.2011.333 (2011). [PubMed: 21946563]

Methods References:

56. Ruggeri ZM, Orje JN, Habermann R, Federici AB & Reininger AJ Activation-independent platelet adhesion and aggregation under elevated shear stress. Blood 108, 1903–1910, doi:10.1182/blood-2006-04-011551 (2006). [PubMed: 16772609]

57. Jakobsen E, Ly B & Kierulf P Incorporation of fibrinogen into soluble fibrin complexes. Thrombosis research 4, 499–507 (1974). [PubMed: 4428463]

58. Thinn AMM et al. Autonomous conformational regulation of beta3 integrin and the conformation-dependent property of HPA-1a alloantibodies. Proceedings of the National Academy of Sciences of the United States of America 115, E9105–E9114, doi:10.1073/pnas.1806205115 (2018). [PubMed: 30209215]

59. Nesbitt WS, Tovar-Lopez FJ, Westein E, Harper IS & Jackson SP A multimode-TIRFM and microfluidic technique to examine platelet adhesion dynamics. Methods in molecular biology 1046, 39–58, doi:10.1007/978-1-62703-538-5_3 (2013). [PubMed: 23868581]

60. Chen Y et al. Fluorescence Biomembrane Force Probe: Concurrent Quantitation of Receptor-ligand Kinetics and Binding-induced Intracellular Signaling on a Single Cell. Journal of visualized experiments, e52975, doi:10.3791/52975 (2015). [PubMed: 26274371]

61. Ju L, Dong J-F, Cruz MA & Zhu C The N-terminal flanking region of the A1 domain regulates the force-dependent binding of von Willebrand factor to platelet glycoprotein Ibα. The Journal of biological chemistry 288, 32289–32301, doi:10.1074/jbc.M113.504001 (2013). [PubMed: 24062306]

62. Ju L & Zhu C Benchmarks of Biomembrane Force Probe Spring Constant Models. Biophysical journal 113, 2842–2845, doi:10.1016/j.bpj.2017.10.013 (2017). [PubMed: 29262376]

63. Chen W, Lou J & Zhu C Forcing switch from short- to intermediate- and long-lived states of the alphaA domain generates LFA-1/ICAM-1 catch bonds. The Journal of biological chemistry 285, 35967–35978, doi:10.1074/jbc.M110.155770 (2010). [PubMed: 20819952]

64. Chen Y, Lee H, Tong H, Schwartz M & Zhu C Force regulated conformational change of integrin alphaVbeta3. Matrix biology 60–61, 70–85, doi:10.1016/j.matbio.2016.07.002 (2017).

65. Liu B, Chen W, Evavold BD & Zhu C Accumulation of dynamic catch bonds between TCR and agonist peptide-MHC triggers T cell signaling. Cell 157, 357–368, doi:10.1016/j.cell.2014.02.053 (2014). [PubMed: 24725404]

66. Williams TE, Nagarajan S, Selvaraj P & Zhu C Concurrent and independent binding of Fcgamma receptors IIa and IIIb to surface-bound IgG. Biophysical journal 79, 1867–1875, doi:10.1016/S0006-3495(00)76436-8 (2000). [PubMed: 11023892]

67. Zhou F, Chen Y, Felner EI, Zhu C & Lu H Microfluidic auto-alignment of protein patterns for dissecting multi-receptor crosstalk in platelets. Lab on a chip, doi:10.1039/c8lc00464a (2018).

68. Kendall MG A New Measure of Rank Correlation. Biometrika 30, 81–93 (1938).

69. Chow GC Tests of equality between sets of coefficients in two linear regressions. Econometrica 28, 591–605 (1960).

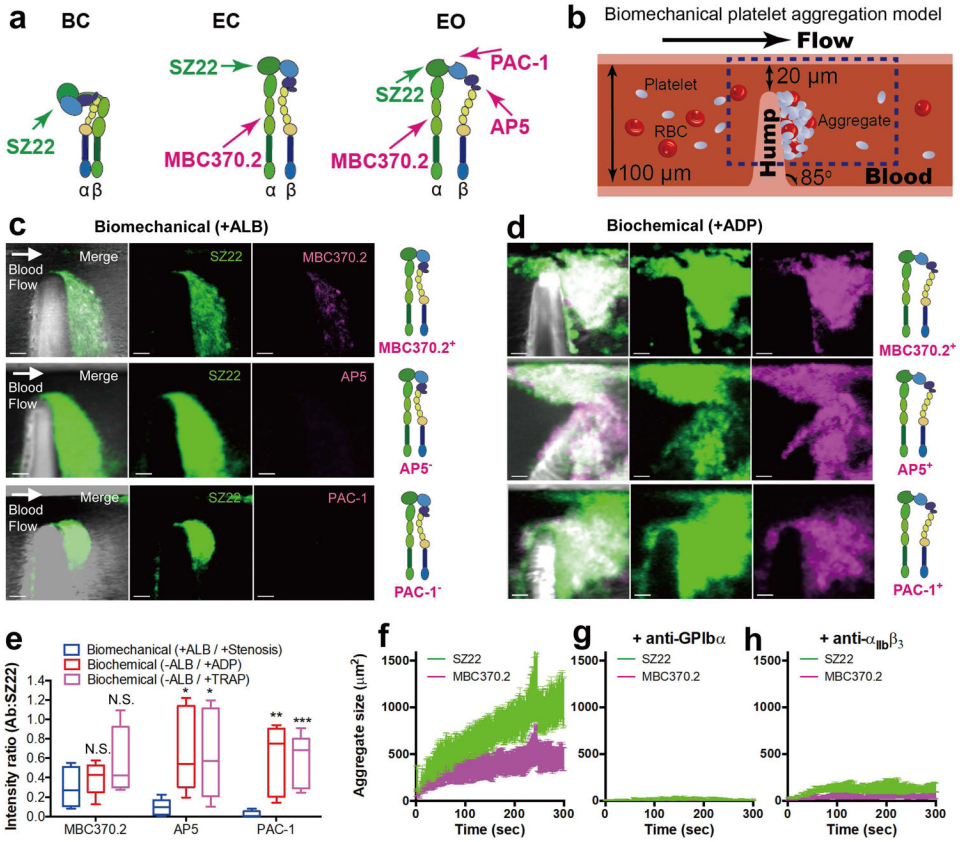

Figure 1. Mapping $\alpha_{IIb}\beta_3$ conformations on platelet aggregates.

(**a**) Current model of three $\alpha_{IIb}\beta_3$ conformations: BC: bent-closed, EC: extended-closed and EO: extended-open. In the EO integrin, the oval notch spanning parts of βI and β-propeller domains indicates the high-affinity ligand binding state recognizable by PAC-1. The binding sites for $\alpha_{IIb}\beta_3$ conformation dependent (MBC370.2, AP5, PAC-1), and independent (SZ22) mAbs were indicated. (**b**) Biomechanical platelet aggregation model showing dimensions of microfluidic channel, inbuilt stenosis hump and platelet accumulation and imaging area (*dashed box*). (**c,d**) Blood was mixed with SZ22-Alexa488 and either MBC370.2-, AP5-, or PAC-1-Alexa647, and perfused through the microfluidic channels at 1,800 s^{-1} bulk shear rate for 10 min. DIC and confocal images were taken to show platelet aggregates and mAb binding (*1st column*: merge; *2nd column*: SZ22; *3rd column*: MBC370.2 (*top*), AP5 (*middle*), PAC-1 (*bottom*)). Biomechanical (*c*) or biochemical (*d*) platelet aggregations were induced by treating blood with amplification loop blockers (ALB) (*c*) or without ALB but adding 50 μM ADP 2 min after platelets start to aggregate on the stenosis downstream (*d*). Images are representatives of ≥3 independent experiments of different human donors in duplicates. Scale bars = 10 μm. (**e**) Quantitation of $\alpha_{IIb}\beta_3$ reporter mAb binding (intensity ratio of reporter mAb over SZ22) upon biomechanical and biochemical stimulations. Data are presented as median ± 25^{th}/75^{th} percentile and min/max values (from left to right, n = 7, 7, 8, 14, 7, 7, 8, 7, 8). N.S. = not significant; *$p < 0.05$; **$p < 0.01$; ***$p < 0.001$, assessed by unpaired t-test with Welch's correction. (**f-h**) Mean ± s.e.m. of $SZ22^+$ and $MBC370.2^+$ areas on platelet aggregates at indicated perfusion time without (*h*) or with 50 μg/ml ALMA12 (*f*) or 20 μg/ml Abciximab (*g*).

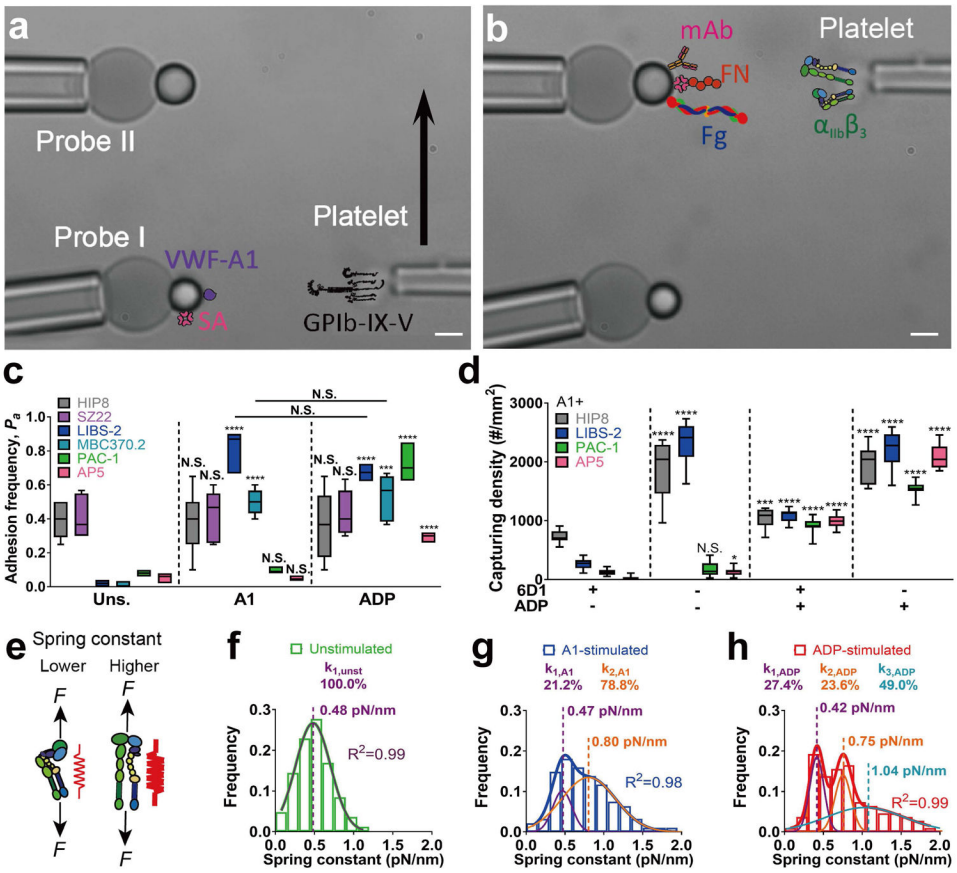

Figure 2. $\alpha_{IIb}\beta_3$ conformational changes following GPIbα signaling and agonist stimulation.

(**a,b**) dBFP setup showing micrographs of a platelet (superimposed with the molecules in question) first aligned with the VWF-A1 bearing probe I (*a*), and then the FN-, Fg- or mAb-bearing probe II (*b*). Scale bars = 2 μm. (**c**) Adhesion frequency of indicated mAbs (median ± 25th/75th percentile and min/max, n = 12) to platelets either unstimulated (*Uns.*), or stimulated by A1 (>2-s lifetime event at 25 pN) or ADP (50 μM, 15 min). (**d**) Number of captured platelets per area of surface co-functionalized with A1 and indicated mAb (median ± 25th/75th percentile and min/max; n = 8, 9, 12, 9, 9, 12, 11, 11, 10, 13, 11, 13, 9, 10, 9, 11) of washed platelets perfused at 4 dynes/cm^2. For each mAb, statistical comparisons in (*c,d*) were made between the current and leftmost condition, *Uns.* in (*c*) and *6D1$^+$ADP$^-$* in (*d*), unless otherwise specified. N.S. = not significant; *p < 0.05; **p < 0.01; ***p < 0.001; ****p < 0.0001, assessed by unpaired, two-tailed Student's t-test. (**e**) Integrin modeled mechanically as a spring under pulling, which has a smaller or larger spring constant, k_{mol}, when it is bent (*left*) or extended (*right*). (**f-h**) Histograms (*bars*) and single (*f*), dual (*g*), or triple (*h*) Gaussian fits (*thin curves*) to the first (*left*), second (*middle*), third (*right*) sub-populations, and overall fits to the whole populations (*color-matched thick curves*) of 160, 181 and 193 k_{mol} measurements respectively on unstimulated (*f*), A1-stimulated (*g*) and ADP-stimulated (*h*) platelets pulled by FN (at ~20% adhesion frequency to ensure mostly single bonds). Portions of some curves are obscured due to overlapping. Goodness-of-fit (R^2) and the fitted mean k_{mol} & fraction of each sub-population were indicated. 10 μg/ml LM609 was added to block $\alpha_V\beta_3$.

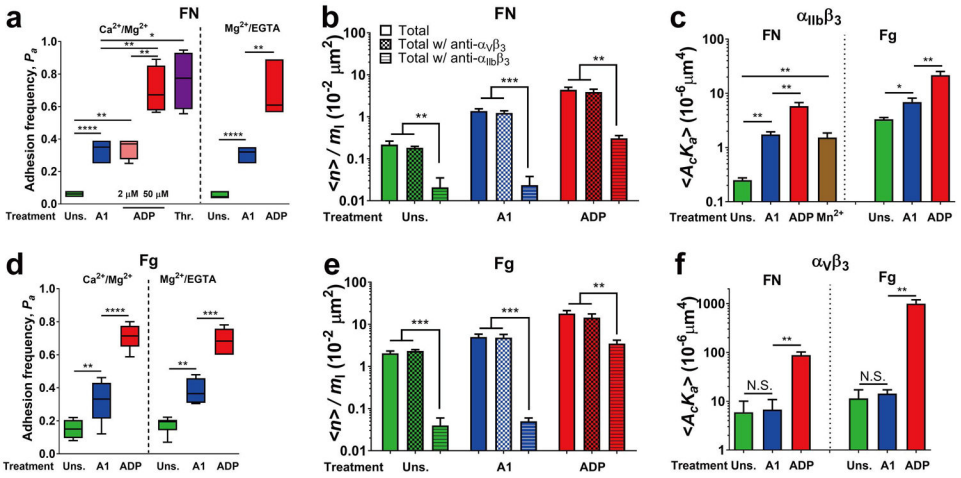

Figure 3. Distinct β_3 integrin activations by GPIbα signaling and soluble agonist stimulation.

(**a**,**d**) Adhesion frequency (P_a) to FN (*a*) and Fg (*d*) of platelets (median ± 25^{th}/75^{th} percentile and min/max, $n = 12$) unstimulated or stimulated by a 25-pN durable (>2-s) force on a GPIbα–A1 bond, by 2 μM (only in *a*) or 50 μM ADP, or by 0.1 U/ml thrombin (only in *a*), in the presence of Ca^{2+}/Mg^{2+} (*left*) or Mg^{2+}/EGTA (*right*; EGTA chelates extracellular Ca^{2+}). The site densities of FN and Fg on the probe beads were 28 and 8 μm^{-2}, respectively. (**b**,**e**) The number of bonds formed between platelets and FN (*b*) or Fg (*e*) beads normalized by the ligand density (mean ± s.e.m., $n = 12$). Bonds were formed by both β_3 integrins capable of binding FN and Fg (*Total*), $\alpha_{IIb}\beta_3$ alone [*Total w/ anti-*$\alpha_V\beta_3$ (LM609)] or $\alpha_V\beta_3$ alone [*Total w/ anti-*$\alpha_{IIb}\beta_3$ (10E5)]. (**c**,**f**) Mean ± s.e.m. of average effective 2D affinity of $\alpha_{IIb}\beta_3$ (*c*) and $\alpha_V\beta_3$ (*f*) binding to FN (*left*) and Fg (*right*). N.S. = not significant; $^{*}p < 0.05$; $^{**}p < 0.01$; $^{***}p < 0.001$; $^{****}p < 0.0001$, assessed by unpaired, two-tailed Student's t-test.

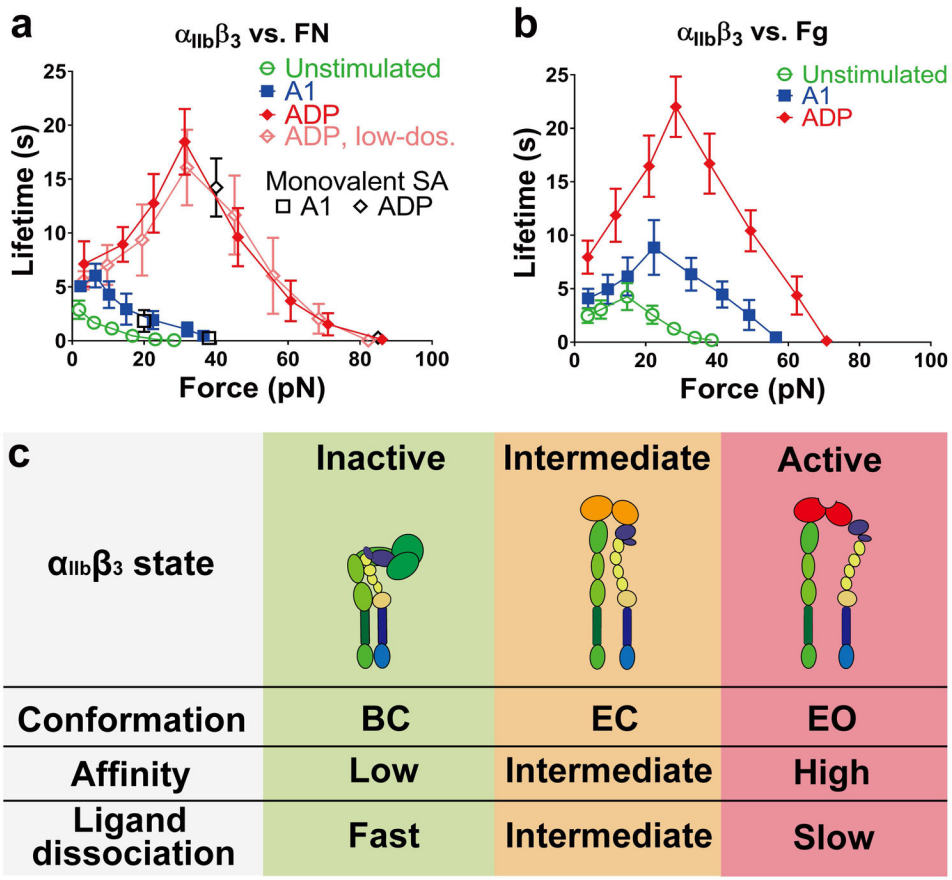

Figure 4. Relation between $\alpha_{IIb}\beta_3$'s activation state and its force-regulated ligand dissociation.

(**a**,**b**) Bond lifetime (mean ± s.e.m) versus force plots ($n \geq 50$ per force bin) of unstimulated (*a*: $n = 330$; *b*: $n = 441$), A1-stimulated (*a*: $n = 379$; *b*: $n = 488$), and 2 μM (only in *a*; $n = 456$) or 50 μM ADP-stimulated (*a*: $n = 435$; *b*: $n = 409$) platelets binding to FN (*a*) or Fg (*b*) in the presence of Ca^{2+}/Mg^{2+}. LM609 was added to block $\alpha_V\beta_3$. Adhesion frequency was adjusted to ~20% to ensure that binding was mediated mostly by single bonds. The lifetimes of $\alpha_{IIb}\beta_3$ bonding to FN captured by monovalent SA measured on A1- and ADP-stimulated platelets (two forces each) were shown in (*a*) for comparison with other data that were obtained using tetravalent SA. (**c**) Summary of three $\alpha_{IIb}\beta_3$ states (inactive, intermediate and active) as characterized by conformation (BC, EC and EO), affinity (low, intermediate, high) and ligand dissociation rate (fast, intermediate, slow). Three colors on the integrin βI and β-propeller domains indicate the three affinity states.

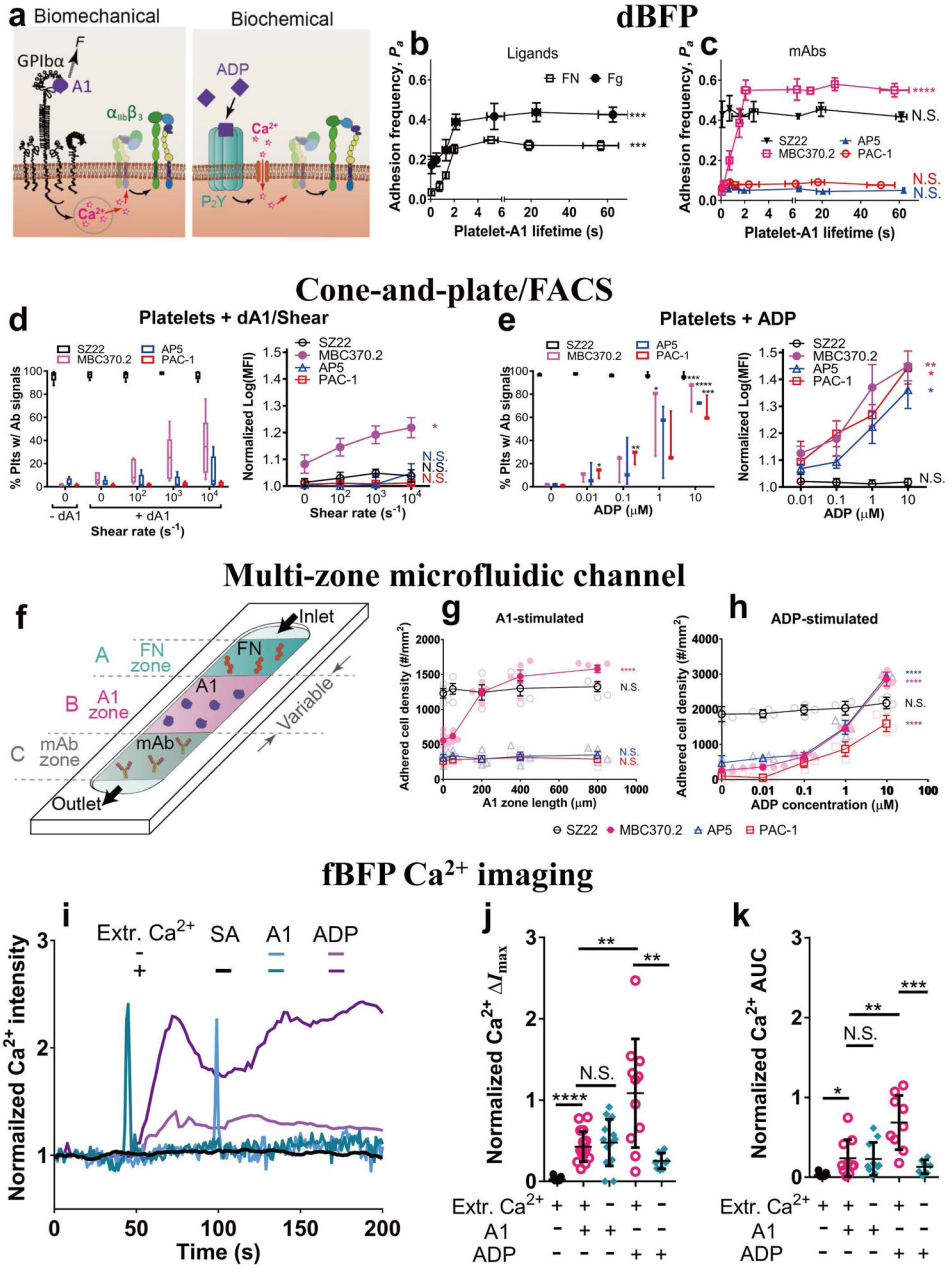

Figure 5. Dose-dependent mechanical and chemical activation of $\alpha_{IIb}\beta_3$.

(**a**) Cartoons depicting biomechanical (*left*) and biochemical (*right*) activation of $\alpha_{IIb}\beta_3$ by A1 and ADP via their respective receptors. (**b**,**c**) Adhesion frequency between FN or Fg (*b*) or indicated mAbs (*c*) and platelets pre-stimulated by a 25-pN GPIbα–A1 bond of indicated lifetime (mean ± s.e.m. for both *x* and *y* variables, $n \geq 9$). LM609 was added to block $\alpha_V\beta_3$. (**d**,**e**) dA1-induced platelet binding by indicated mAbs in a cone-and-plate rheometer at indicated shear rates (*d*) or ADP concentrations (*e*). Results ($n \geq 3$) are either percentage of platelets with mAb staining (*left*; median ± 25th/75th percentile and min/max; groups compared by unpaired, two-tailed Student's t-test) or logarithmized median fluorescence intensities normalized by untreated platelets (*right*; mean ± s.e.m.). (**f**) Schematic of the

multi-zone microfluidic channel. (**g**,**h**) Mean ± s.e.m. ($n \geq 4$) platelet density on the indicated mAb zone after stimulated by A1 zone of variable lengths (multi-zone channel; *g*) or ADP of different concentrations (single-zone channel; *h*). In *b*, *c*, *d* (*right*), *e (right)*, *g* and *h*, one-way ANOVA was used to access whether the points in the same curve were significantly different (Supplementary Table 3a). (**i**) Representative single-cell intraplatelet Ca^{2+} signals following A1 or ADP stimulation in Ca^{2+}/Mg^{2+} (Extr. Ca^{2+} = "+") or Mg^{2+}/EGTA (Extr. Ca^{2+} = "−"). SA-coated beads were used as a control for A1-stimulated condition. (**j**,**k**) Maximum increase (ΔI_{max}) (*j*) and area-under-curve (AUC) (*k*) of platelet Ca^{2+} signals (points and mean ± S.D.) under indicated conditions (groups compared by unpaired, two-tailed Student's t-test; n = 13, 17, 15, 11, 9). N.S. = not significant; $^{*}p < 0.05$; $^{**}p < 0.01$; $^{***}p < 0.001$; $^{****}p < 0.0001$.

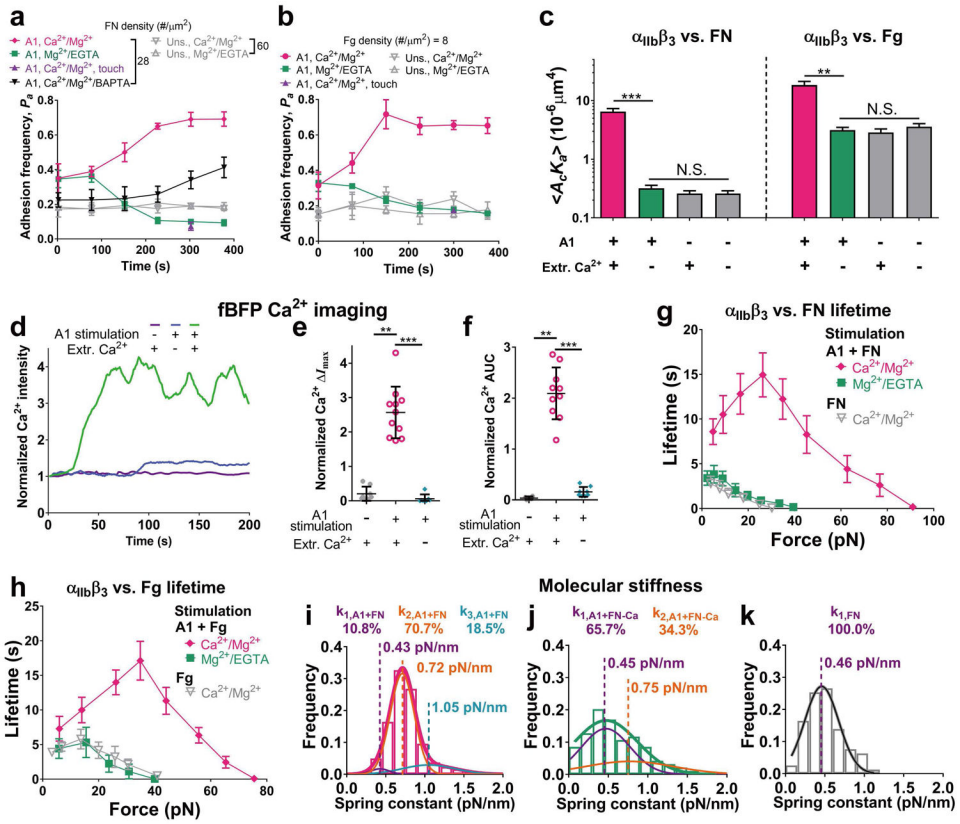

Figure 6. Mechanical affinity maturation of intermediate state $\alpha_{IIb}\beta_3$.

(**a,b**) Platelet adhesion frequency (of every 30 touches) to FN (*a*) or Fg (*b*) with (*filled symbols*) or without (*open symbols*) A1 pre-stimulation over 180 repeated touches (2.5-s/touch) (mean ± s.e.m., $n = 9$). *Filled triangle*: adhesion frequency to FN (*a*) or Fg (*b*) of A1-stimulated platelets after 300-s continuous contact without pulling. (**c**) $\langle A_c K_a \rangle$ (mean ± s.e.m.) of $\alpha_{IIb}\beta_3$–FN or $\alpha_{IIb}\beta_3$–Fg binding after 100 repeated touches with or without A1 pre-stimulation in the presence (+) or absence (−) of extracellular Ca^{2+}, estimated from the last point of corresponding curves in (*a,b*). (**d-f**) Representative curves (*d*) and ΔI_{max} (*e*) and AUC (*f*) (individual platelets and mean ± S.D.; $n = 9, 11, 9$) of intraplatelet Ca^{2+} signals during repeated FN pulling in Ca^{2+}/Mg^{2+} (Extr Ca^{2+} = "+") or Mg^{2+}/EGTA (Extr Ca^{2+} = "−") with A1 pre-stimulation, or in Ca^{2+}/Mg^{2+} without A1 pre-stimulation. (**g,h**) $\alpha_{IIb}\beta_3$–FN (*g*) and $\alpha_{IIb}\beta_3$–Fg (*h*) bond lifetimes (mean ± s.e.m.) measured after 100 contacts to A1 pre-stimulated platelets in Ca^{2+}/Mg^{2+} (*g*: $n = 468$; *h*: $n = 598$) or Mg^{2+}/EGTA (*g*: $n = 408$; *h*: $n = 285$), or for platelets without A1 pre-stimulation in Ca^{2+}/Mg^{2+} (*g*: $n = 311$; *h*: $n = 348$) ($n \geq 50$ per force bin). (**i-k**) Histograms and triple (*i*), dual (*j*) or single (*k*) Gaussian fits of 192, 172 and 166 k_{mol} measurements respectively on platelets pre-stimulated by A1 in Ca^{2+}/Mg^{2+} (*i*) or Mg^{2+}/EGTA (*j*), and platelets without A1 pre-stimulation in Ca^{2+}/Mg^{2+} (*k*). R^2, fitted mean k_{mol} and fraction of each sub-population were indicated. LM609 was added in all experiments. N.S. = not significant; $^{**}p < 0.01$; $^{***}p < 0.001$, assessed by unpaired, two-tailed Student's t-test.